GROUND INFLUENCE ON HIGH-PRESSURE METHANE JETS: PRACTICAL TOOLS FOR RISK ASSESSMENT

Cristian Colombini, Andrea Martani, Renato Rota, Valentina Busini*

Politecnico di Milano - Department of Chemistry, Materials and Chemical Engineering "Giulio Natta", Piazza Leonardo da Vinci 32, 20133, Milano, Italy

* Corresponding author:

E-mail address: valentina.busini@polimi.it

ABSTRACT

High-pressure gaseous methane release is a relevant safety-related problem mainly in the Oil and Gas industry. As well documented, the reason for these safety concerns is connected with the severe consequences of the domino effect subsequent to the possible ignition. In risk assessment activities, estimation of the damage area is of primary importance in order to draw up proper safety guidelines. To do this, loss prevention specialists use quick and well-established numerical tools (i.e., integral models) in their daily activities. However, the presence of an obstacle in the flow field of the jet (e.g., the ground) is a more probable situation to deal with. It is known that integral models fail in this kind of scenario, leading to unreliable predictions. Hence, the present work investigates how an industrial ground surface influences the LFL cloud size of a horizontal high-pressure methane jet. An innovative quick procedure is proposed allowing to determine the height below which the ground begins to influence the LFL cloud size and the extent of such influence. Therefore, this procedure allows practitioners to establish when integral models can be used and when not to use them, and also provides a simple and reliable alternative to their use. These analytical instruments are derived from an extensive computational fluid dynamics analysis performed with Ansys Fluent 19.0.

KEYWORDS

High-pressure release; methane; ground influence; risk assessment; CFD; analytical correlation

ACRONYMS

CFD Computational Fluid Dynamics

HPJ High Pressure Jet

LFL Lower Flammability Limit

ME Maximum Extent

QRA Quantitative Risk Analysis

UDF User Defined Function

NOMENCLATURE

a: virtual orifice displacement

C_D: discharge coefficient

d: actual orifice diameter

d_{PS}: pseudo-source orifice diameter

h: height of the source above ground

h*: critical height of the source above ground

k: axial decay constant

ME: LFL cloud maximum extent in direction of the jet axis

ME_{FJ}: free jet LFL cloud maximum extent in direction of the jet axis

ME_X: maximum lateral extent of the LFL jet cloud

p: storage pressure

p_{amb}: environmental pressure

T: storage temperature

T_{amb}: environmental static temperature

v_Z: wind velocity component parallel to the jet axis

z: downstream distance

Δ: percentage variation of ME with respect to ME of the free jet

γ: specific heat ratio

η: axial mole fraction

ρ_a: air density

ρ_g: methane density

1. INTRODUCTION

Although transporting and storing of chemicals under liquefied conditions (obtained through compression or cooling) is widespread, many of them are still handled in gaseous form (Kim et al., 2013; Bariha et al., 2017; Deng et al., 2018; Baalisampang et al., 2019; Lim et al., 2019; Stewart, 2019).

Therefore, from the industrial safety point of view, the risk assessment of accidental toxic or flammable high-pressure gaseous releases (*i.e.*, High-Pressure Jets, HPJ) is a critical challenge, especially for Quantitative Risk Analysis (QRA) and in the hazardous area classification framework (Pontiggia et al., 2014; Liao et al., 2018).

Regardless of the kind of substance involved, generally the safety evaluation mainly involves estimation of the hazardous area connected (Souza et al., 2019).

Concerning the flammable case, if an ignition takes place, the possible consequences of a leak can be considerable (Bariha et al., 2017; Kong et al., 2019; Pu et al., 2019; Tolias et al., 2019; Yang et al., 2020): due to the domino effect, flash fires and jet fires are among the most hazardous accidents (Benard et al., 2009; Casal et al, 2012; Zhou et al., 2018).

In general, the safety evaluation related to the accidental discharge of flammable materials can be performed by determining the Maximum axially-oriented Extent (ME) of the flammable cloud (Tchouvelev et al., 2007; Houf et al., 2010; Pontiggia et al., 2014; Colombini and Busini, 2019a; Colombini and Busini, 2019b).

Thinking of a realistic industrial situation where a high-pressure flammable jet may occur, it is quite evident that the flammable cloud may interact with equipment or structures (Xu et al., 2011).

In this case the jet development can be influenced by interaction with an obstacle (Tchouvelev et al., 2007; Benard et al., 2009; Middha et al., 2010; Kotchourko et al., 2014): in principle, the enhanced turbulence effects on one hand (that increases the entrainment of fresh air, leading to a faster dilution of the hazardous substance) and the reduction of momentum on the other hand (inducing a lower turbulence level that can lead to an increase in the critical area involved) suggest that from the industrial safety point of view the obstacle could affect the jet behaviour either positively or negatively. Therefore, with respect to the free jet scenario (intended as a release occurring in an unconfined environment (Dey et al., 2017)), which is the most common situation considered in the industrial safety practice (Dasgotra et al., 2018), in some cases the effect can be an increase in the hazardous area involved, *i.e.*, the ME of the jet cloud is larger than that of a free jet, while in other cases it can be lower (Kotchourko et al., 2014; Hall et al., 2017).

As for accidental scenarios involving low momentum spills of hazardous gases (*e.g.,* cloud dispersions from liquid pools), in the presence of any kind of obstacle, integral models can give unreliable results (Cameron and Raman, 2005; Schelder et al., 2015; Gerbec et al., 2017; Uggenti et al., 2017; Dasgotra et al., 2018).

The main reason why this kind of numerical model usually fails to reproduce accidental releases in complex geometries is that integral models account for some physical phenomena through semi empirical correlations having parameters that have been fitted to some field test data (Derudi et al., 2014). Their accuracy is therefore strictly related to the experimental tests used to tune the model parameters. Given that obstacles are not usually present in such field trials, it is easy to understand how the integral models give reliable predictions only for free jet scenarios.

To the best of Authors' knowledge, although improvements have been made in recent years concerning low-computational-cost tools in the framework of accidental releases risk assessment, the previously highlighted limits of the integral models in reproducing complex geometry situations are still present.

Therefore, simulation models developed in the frame of Computational Fluid Dynamics (CFD) need to be used (Batt et al., 2016; Alves et al., 2019). The reason is that only a distributed parameter model can address a problem at any level of geometrical complexity (Efthimiou et al., 2017; Gerbec et al., 2017; Luo et al., 2018; Jiang et al., 2020), providing the user with detailed qualitative

and quantitative information on the flow field (Cameron and Raman, 2005; Deng et al., 2018; Luo et al., 2018; Tolias et al., 2019). However, this approach is not yet free of drawbacks: the amount of resources needed, both in terms of computational costs and analyst skills required, still limits its use (Jiang et al., 2020).

Falling under the general definition of an obstacle, flat surfaces close to the jet source, such as the ground or vertical walls, are of particular interest in the industrial safety field since they can induce an enlargement of the hazardous area (Benard et al., 2007; Benard et al., 2009; Desilets et al., 2009; Hourri et al., 2009; Hourri et al., 2011; Angers et al., 2011; Kotchourko et al., 2014; Benard et al., 2016; Hall et al., 2017).

In particular, in 2007 Benard and co-workers numerically investigated the influence of vertical and horizontal flat surfaces parallel to unignited vertical and horizontal hydrogen and methane HPJ. They performed the study considering a single reservoir pressure value (284 bar), a specific orifice dimension (8.5 mm) and a fixed distance of the jet source from the surface (1 m). The results showed that in spite of the high-momentum of the releases, the ME of hydrogen jets is strongly influenced by the buoyancy effect, while the ME of methane jets is not. Starting from this work, Hourri et al. (2009) included two more distances of the jet source from the surface (0.5 and 2 m). Benard et al. (2009) considered horizontal releases occurring from an orifice with a different diameter (6.35 mm), from two different storage pressure values (100 and 700 barg) and several distances from the surface (from 0.1 to 10 m). Hourri et al. (2011) investigated different storage pressures (250, 400 and 550 barg), while, Angers et al. (2011) extended the analysis done by Hourri et al. (2011) to the case of vertical jets. Benard et al. (2016) combined the results of some of these works establishing engineering correlations to quantify the flammable extent of both hydrogen and methane jet releases.

Limited to hydrogen releases, some empirical information is also available: Desilets et al. (2009) performed a series of laboratory experiments on the LFL cloud extension considering two storage pressures (6.6 and 16.3 bar), two orifice diameters (1.6 and 0.79 mm), and several distances from the horizontal adjacent surface (1-30 cm), Hall et al. (2017) reported empirical data for two storage pressure values (150 and 425 barg) through nozzles with a diameter of 0.64 and 1.06 mm, respectively. The focus was on understanding how horizontal surfaces influence the releases of both unignited and ignited hydrogen.

As a matter of fact, the methane high-pressure gaseous release is a relevant safety-related problem mainly in the Oil and Gas (O&G) industry. The reason for its importance is related to the

severe consequences of the subsequent domino effect that may take place if ignition of the release occurs, either immediately (jet fire) or with a delay (flash fire). In risk assessment the damage area of the jet cloud (in particular, the hazardous distance reached by the LFL concentration value) is recognised as the characteristic distance of interest in the risk analysis process. To estimate the maximum axially-oriented extent of the flammable cloud, in their daily activities loss prevention specialists use quick and well-established numerical tools such as integral models (*e.g.*, PHAST (DNV, 2020)). However, the presence of an obstacle in the flow field of the jet is a more realistic situation to deal with. Therefore, the main aim of the present work is to investigate how an industrial ground surface (*i.e.*, made of concrete) can influence the LFL cloud size of a horizontal high-pressure methane jet through an extensive CFD analysis performed with Ansys Fluent 19.0. The main innovative aspect of this work is a quick procedure making it possible to i) determine the minimum height from which the ground begins to influence the hazardous distance; since below this height the predictions of standard simulation tools are not reliable and a simple tool allowing practitioners to know whether or not a given accidental scenario can be simulated with standard modelling tools is of paramount practical importance, and ii) estimate how much the hazardous distance increases when the ground influence makes the predictions of the standard simulation tools unreliable.

The paper outline is the following: at first, key methodological aspects of the CFD model developed are discussed; then, referring to a selected case among the various analysed, the proposed criterion and the derived analytical correlation are discussed in detail. Therefore, the reliability of the proposed approach is investigated by comparison with the CFD results of many realistic scenarios (nearly 250 cases). Finally, a simple way to use the proposed methodology independently from any CFD computation is suggested and compared with the previous results. In the conclusions, an overall simple procedure is presented that allows safety analysts to estimate by hand the hazardous distance.

2. MATERIALS AND METHODS

Thanks to the capabilities of bring-together and easy-to-use design, to perform the present CFD numerical analysis the Ansys Workbench suite (v. 19.0) was used. A particular aspect that has to be

highlighted about this software suite is the possibility of easy design and parametric analysis study.

The geometry domain was created with Ansys DesignModeler software, the grid was built using Ansys Meshing and the computations were undertaken with the numerical solver Ansys Fluent. Description of the Workbench platform and the three specific software used is extensively reported in the corresponding owner User Guides (Ansys DesignModeler User Guide, 2017; Ansys Meshing User Guide, 2017; Ansys Fluent User Guide, 2017). Reasons, kinds and values of all the CFD analysis settings are reported and described in detail in the next Section of the paper.

With the aim of avoiding the need to simulate the early stage of the jet development (*i.e.*, the so-called nearfield zone of the jet), the use of a fictitious jet source makes it possible to save computational costs keeping the reliability of the results within an acceptable range (in particular, if the farfield zone of the jet is of primary interest). Named in several ways, such as equivalent diameter, notional nozzle, pseudo-source or fictional nozzle (Franquet et al., 2015), this widely adopted kind of approach was used to model the jet source term as discussed in the following Section.

3. RESULTS AND DISCUSSION

Further below the base case scenario analysis is discussed with particular reference to the definition of the physical scenario, the setup of the CFD analysis in each of its steps and the results of the analysis. Then the parametric analysis conducted is outlined and the main results are discussed. As a last step, with the double aim of further validating the CFD model and making the analytical tools proposed more usable for on-field assessments, a comparison with the results obtained exploiting a simpler tool than CFD is presented for the free jet situation.

3.1 BASE CASE SCENARIO

The base case scenario was a realistic situation of industrial interest involving an accidental horizontally oriented high-pressure release of methane adjacent to the ground. Assuming a release from a storage tank (or a pipeline) sufficiently large, the loss of containment can be treated as stationary. Referring to the scenario considered in the work of Colombini and Busini

(2019a), a pressure of 65 bara and a temperature of 278 K were considered as upstream gas conditions. A one-inch diameter hole was assumed as a possible accidental orifice (Hendrickson et al., 2015). Since the scenario is outdoors, and the purpose of this work is risk-assessment oriented, the analysis was conducted considering the 5D atmospheric stability class (*i.e*., a wind intensity of 5 m/s at 10 m from the ground and a Pasquill stability class of D) (Pontiggia et al., 2009). In particular, the worst case situation of wind blowing alongside and in the same direction of the jet was taken as reference and adopted in all the simulations. As regards the flat surface adjacent to the release, a concrete ground surface was assumed as the kind of terrain that can be more often found in an industrial plant.

Hence the base case scenario was set as an array of situations defined by different heights of the source above ground (namely 13 cases, from 14.5 cm to 4.3 m).

3.1.1 CFD MODEL DEFINITION

As described in Section 2, the jet source term was modelled through the use of an equivalent diameter model instead of considering the actual source term. In defining the geometry this meant that the hole diameter to be considered was based on the equivalent diameter model adopted (and the upstream conditions). In the present work the model developed by Birch et al. (1984) was chosen, leading to a pseudo-source diameter of 14.58 cm (*i.e.*, almost 6 times the actual one). It is worth mentioning that because the farfield zone of the jet is of primary interest in this work and according to the work of Crist et al. (1966), the axial displacement of the pseudo-source from the actual one, a, was neglected.

The computational domain extents were sized similarly to the work of Hourri et al. (2009). Since the ground can only increase the ME of the jet cloud, to avoid any boundary interference on the jet cloud development the domain extents were sized considering the worst-case scenario (*i.e.*, the lower h) (Tolias et al., 2019). Thus the computational domain was a rectangular box of 100 m length, 25 m height and 10 m wide (when a symmetry plane is adopted, while 20 m when the full 3D geometry is considered).

The domain was discretised using five virtual line bodies splitting the jet axis which served as geometrical base for the Ansys Meshing body of influence feature. As a result, cells thickening within a volume surrounding the jet axis was achieved and less expensive coarse mesh far from the "critical" zone of the domain (*i.e.*, where gradients are expected to be less relevant) was obtained. In Table 1, all the specifics about the body of influence feature for each of the five line

bodies are listed; length and cell size are expressed with respect to the equivalent diameter value allowing to maintain proportionality of the grid specifics when the scenario characteristics, which affect the d_{PS} value, vary. While, Figure 1 shows the computational domain considered for one of the source heights investigated in the base case. In particular, the five line bodies are highlighted in the Figure (core in green, far1 in orange, far2 in light blue, far3 in magenta and far4 in blue). Another constraint on the grid generation was imposed at the jet exit. In particular, the same cell dimension along the jet axis used for the ''core'' line body was adopted.

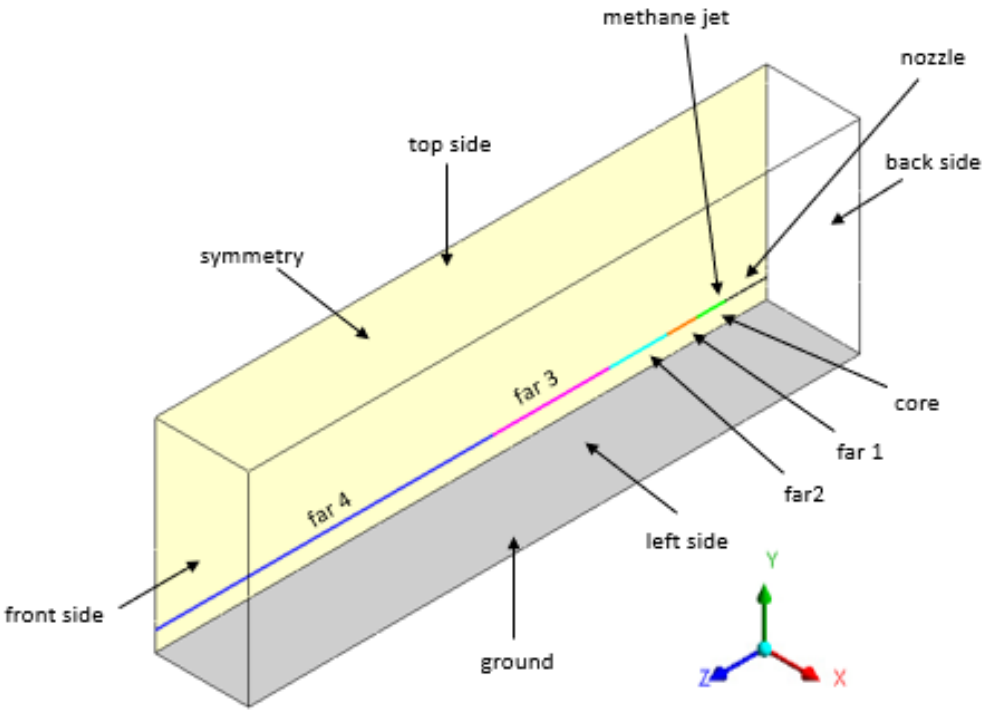

Fig. 1: Sketch of the computational domain for h = 4.374 m.

Table 1: Geometrical and mesh specifics of the five body of influence features used in the base case scenario simulations.

Legend as in Figure 1	Core	Far1	Far2	Far3	Far4
$\frac{Length}{d_{PS}}$ [-]	35	35	70	140	391
$\frac{d_{PS}}{Cell\ size}$ [-]	73	18	10	3	1
Growth rate	1.075	1.1	1.15	1.175	1.2

In this way the fluid domain was discretised using a fully unstructured tetrahedral grid. Figure 2 shows how the whole resulting mesh appears (a) and its detail in proximity to the jet orifice (b). Depending on the height of the source from the ground, the cell count ranged between 7.3 and 7.8 million of elements. Quality requirements in terms of skewness and orthogonal quality were always satisfied. With respect to the independence of the results from the grid, it was checked for a reference case by repeating the simulation twice: with respect to the values reported in Table 1, the elements size of the body of influence features were halved and doubled, respectively. Both qualitatively (in terms of cloud shape) and quantitatively (in terms of concentration decay along the jet centreline), good matching was achieved. Figure 1S in the supplementary material shows the comparison of the sensitivity analysis results in terms of methane mole fraction contours.

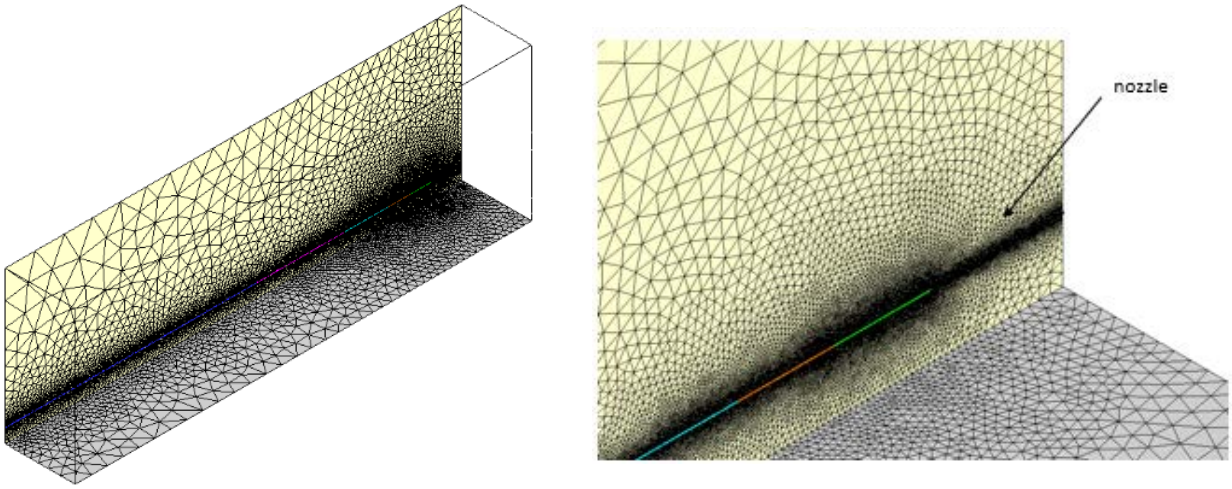

(a) (b)

Fig. 2: Whole grid appearance around the jet centreline (a) and a detail in the surrounding of the orifice (b) for the case of h = 4.374 m.

All the simulations of the base case scenario discussed here (and all those of the sensitivity cases presented later on) were performed in steady state conditions and the pressure-based solver was chosen thanks to the equivalent diameter model deployment (allowing the flow to be treated as incompressible). The Reynolds-averaged approach was employed for the governing Navier-Stokes equations (RANS approach). The two-equation eddy-viscosity k-ω SST turbulence closure model (Menter, 1993) was chosen to account for the turbulence on the flow field avoiding, on the other hand, the need to simulate the boundary layer region precisely next to the ground. To account for the multi-species problem (methane release in ambient air), the species transport model without any kind of reaction was selected and the ideal gas equation of state was used to model the fluid

mixture density. The COUPLED pressure-velocity coupling scheme was adopted while the second order upwind spatial-discretisation scheme was considered for all the convective terms. Table 1S in the supplemental information lists the model equations together with the definition of the main parameters.

Table 2 reports all the characteristics of the methane pseudo-source inlet boundary condition according to the Birch et al. (1984) approach. Table 3 lists all the other boundary conditions together with their specifics, while, Figure 1 shows also their correspondent position in the computational domain. Notice that to properly model the realistic wind conditions of an open field scenario, a velocity profile reproducing the atmospheric class 5*D* was provided through an *ad hoc* User Defined Function (UDF). Gravity acceleration was always included perpendicularly to the ground surface.

Table 2: Pseudo-source characteristics as calculated by the model of Birch et al. (1984) for the base case scenario.

Characteristic	Value
Equivalent diameter	0.145 m
Velocity	440.9 m/s
Mass flow rate	5.184 kg/s
Total temperature	343.8 K
Pressure	101325 Pa

Table 3: Boundary conditions assignments used for the simulations.

Boundary name	Type	Specifics
Back side	Velocity inlet	air, v_z = UDF velocity profile, T = 300 K
Top side	Velocity inlet	air, v_z = 5.5 m/s, T = 300 K
Left side	Velocity inlet	air, v_z = UDF velocity profile, T = 300 K
Ground	Wall	0.01 m roughness height, adiabatic
Symmetry	Symmetry	-
Front side	Pressure outlet	air, $T_{BACKFLOW}$ = 300 K
Nozzle	Wall	0.001 m roughness height, adiabatic
Methane jet	Mass flow inlet	See Table 2

3.1.2 ANALYSIS OF THE RESULTS

To study the effect of the ground on the ME of a horizontally oriented high-pressure release of methane, an analysis varying the height of the jet exit above the ground was performed. The entire set of leak orifice heights simulated (from 1 pseudo diameter up to 30 pseudo diameters above ground) together with the corresponding ME values computed and their percentage variation with respect to the free jet one (Δ_z), are reported in Table 4. Moreover, to remark

quantitatively on the significant difference between the parallel and the normal to the jet axis maximum extent of the LFL jet cloud, the last row of Table 4 lists the Maximum lateral Extent of the LFL jet cloud (ME_X). Notice that the lateral dimensions are related to the symmetry case (*i.e.*, the full lateral extent of the cloud is twice such values). For comparison purposes, the last column (case 13 in the Table) lists the characteristics of the free jet situation. Figure 3 shows the LFL contours for some representative scenarios. Moreover, Figure 2S in the supplemental information shows, for the same cases, contours of temperature, velocity and turbulent kinetic energy.

Table 4: computed values of ME and their percentage variations with respect to the ME of the free jet case for the base case scenario. Last row lists the corresponding MEx of the LFL envelopes.

case	1	2	3	4	5	6	7	8	9	10	11	12	13
h [m]	0.145	0.437	0.729	1.026	1.312	1.604	1.895	2.187	2.479	2.77	3.061	3.353	4.374
h/d_{PS} [-]	1	3	5	7	9	11	13	15	17	19	21	23	30
ME [m]	63.4	51	43.8	37.4	31	22.8	17.05	16.7	16.6	16.5	16.5	16.45	16.45
Δ_z [%]	+285	+210	+166	+127	+88	+38	+3.6	+1.5	+0.9	+0.3	+0.3	+0	+0
ME_X [m]	1.68	1.65	1.63	1.45	1.15	1.08	1.07	1.07	1.07	1.05	1.07	1.05	1.05

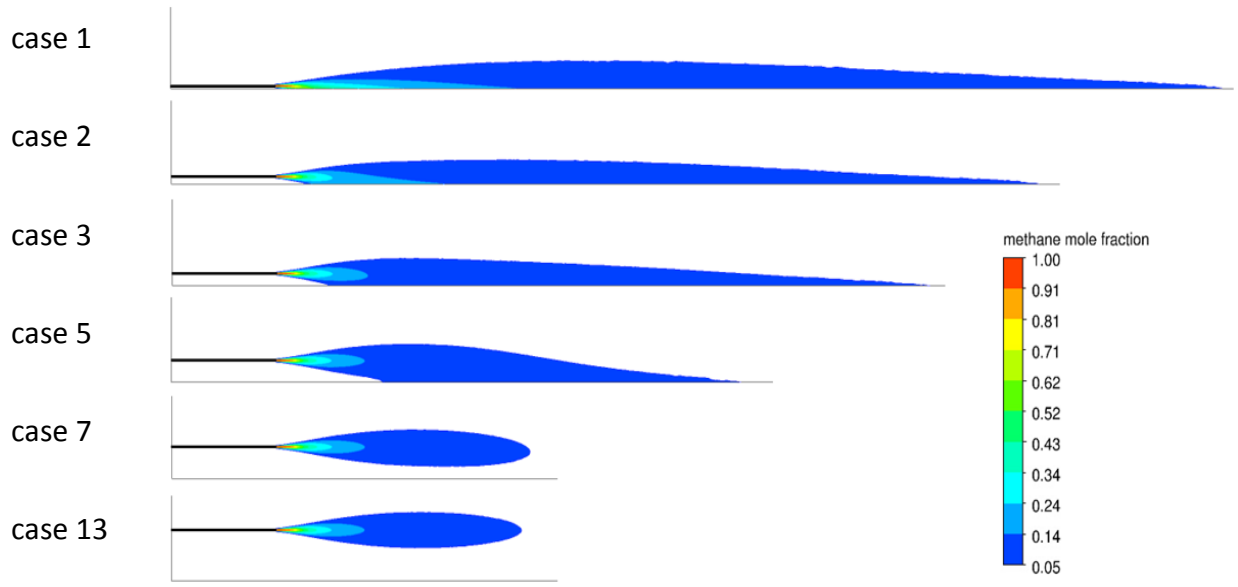

Fig. 3: LFL mole fraction contours of methane in air for some of the heights considered.

From both Figure 3 and Table 4, it can be noted that more the jet exit is close to the ground, the longer the ME is. The fact that for small heights (*i.e.*, in the order of the pseudo-source diameter) the resulting ME of the jet is almost four times the ME of the correspondent free jet underlines the need for the ground presence in safety risk assessments analysis to be carefully accounted for.

From the results shown in Figure 3 we can see that methane jets are momentum dominated. For the various situations investigated, no significant buoyancy effects can be noticed. Moreover, the Coanda effect deviates the jet development towards the ground (Miozzi et al., 2010). This occurs because the ground limits the entrainment of surrounding air causing, with respect to the upper side of the jet, a lower pressure that attracts the jet.

Figure 4 shows how ME varies as a function of the source height above the ground (h). This plot clearly depicts some findings: i) over a specific critical height of the jet above ground (h*), the jet is not influenced by the ground presence (*i.e.*, the ME is equal to the free jet one); ii) once the ground influence is noticed, it acts enhancing the ME of the jet; iii) the overall increase of ME presents an almost inverse linear proportionality to h.

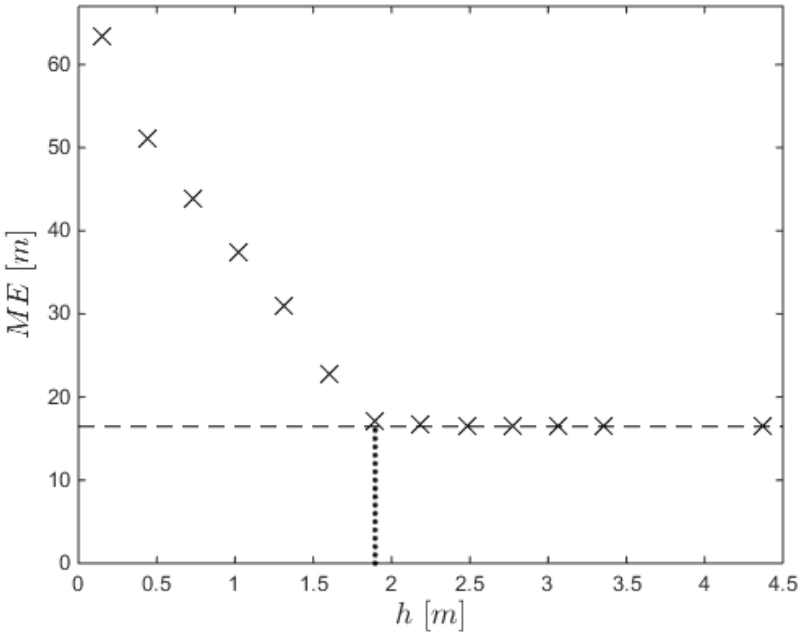

Fig. 4: LFL ME plotted against h for all the cases considered in the base case scenario. In the Figure, the dashed line and the dotted line represent the ME of the free jet case (ME_{FJ} = 16.45 m) and the critical height of the jet above ground (h* = 1.895 m), respectively.

3.1.3 PROPOSED CRITERION AND ANALYTICAL CORRELATION

Although the results previously shown can be expected to be qualitatively valid for different scenarios, they could lack general application for three main reasons:

1. varying the storage pressure, the results might be different in terms of ME
2. a variation of the actual orifice diameter will affect the jet characteristics in some way and therefore even the ME will also be influenced. In fact the orifice diameter directly influences the pseudo-source diameter, as shown by the following equation (Birch et al., 1984):

$$d_{PS} = d\sqrt{C_D\left(\frac{p}{p_{amb}}\right)\left(\frac{2}{\gamma+1}\right)^{\frac{(\gamma+1)}{2(\gamma-1)}}} \quad (1)$$

   where d_{ps} is the resulting diameter of the pseudo-source, d is the actual orifice diameter, C_D is the discharge coefficient, p is the storage pressure, p_{amb} is the environmental pressure and γ is the specific heat ratio
3. Since there are several equivalent diameter models available in literature (Franquet et al., 2015), the choice of a particular model can affect the jet characteristics

To generalise the results reported in Figure 4, they were made dimensionless using the ME value of the free jet case (ME_{FJ}) and the pseudo-source diameter (d_{PS}) as shown in Figure 5. This graph shows how the ME (obtained in each of the cases) varies with respect to ME_{FJ} as function of the height above ground of the jet orifice (h) expressed as the number of pseudo-source diameters (d_{PS}).

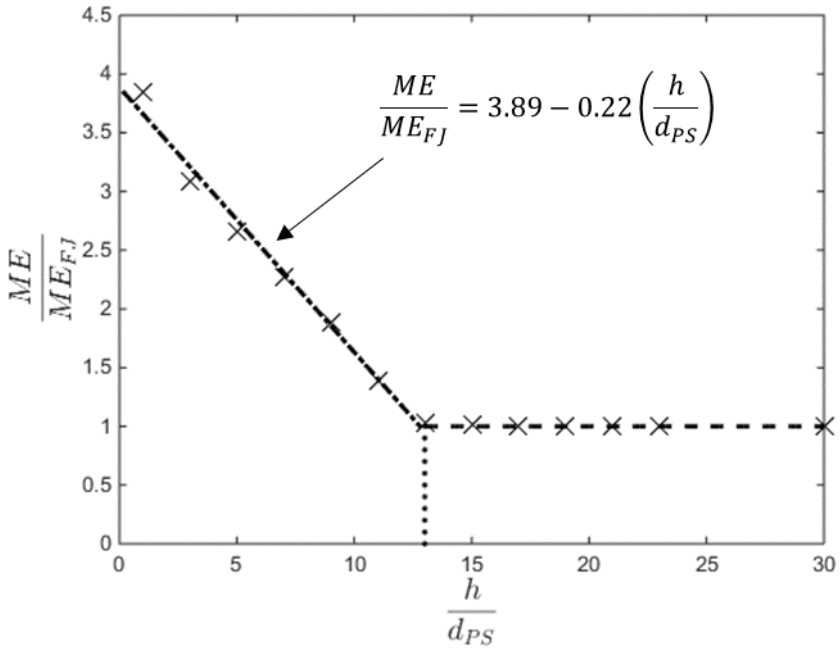

Fig. 5: Dimensionless ME over the dimensionless height of the source above ground for all the cases of the base case scenario. In the Figure, the dashed-dotted line represents the linear fitting of the computed results influenced by the ground, the dashed line represents the linear fitting of the ones not influenced by the ground and, the dotted line represents the critical dimensionless height of the jet above ground (h/d_{PS}* = 13).

From Figure 5 it is possible to: i) determine a threshold value that, in terms of h/d_{PS}, acts as a criterion establishing when the ground effect starts to be noticeable and ii) derive an analytical correlation that makes it possible to assess the increase of the LFL cloud extent due to the ground effect.

With respect to the first point, the h/d_{PS} threshold limit is equal to about 13 while, the first-order polynomial function that best fits the numerical outcomes for $h/d_{PS} < 13$ (with a coefficient of determination equal to 0.988) is

$$\frac{ME}{ME_{FJ}} = 3.89 - 0.22\frac{h}{d_{PS}} \tag{2}$$

3.2 SCENARIO SENSITIVITY ANALYSIS

To investigate the validity of both the threshold criterion and the correlation discussed in the previous Section, a sensitivity analysis considering several realistic scenarios (nearly 250 cases) was performed. First, various source conditions (in terms of storage pressure and actual orifice

diameter) were analysed. Second, three other wind intensities were considered as possible open field conditions in which the jet can occur. Third, two other pseudo-source models were used to determine the source characteristics for the incompressible simulations. Finally, when coherent with the present work, the numerical results of Benard et al. (2016) were included.

The full set of the analysed scenarios is reported in Table 5, while the computed results, in terms of ME as a function of the height above ground of the jet source, are shown in Figure 6.

When required, domain size and cell dimensions of the bodies of influence features were properly resized to contain the whole LFL envelopes in the domain.

Concerning the ME sensitivity dependent on the storage pressure, the minimum value to obtain critical conditions (cases 14-21), halving the value used in the base case scenario (cases 22-29) and doubling it (cases 30-37), was used. From Figure 6.a it is possible to observe that at the same value of h, the higher the storage pressure is, the larger the ME is. This is expected since an increase in the storage pressure leads to an increase in the corresponding equivalent orifice diameter (see Eq. 1) which at constant velocity implies a larger mass flow rate. For the same reason the influence of the terrain starts at different heights; the lower the storage pressure is, the lower the threshold value h* is. However, regardless of the storage pressure value, once the ground influence starts it deviates the jet in the same way. This is why the slope of the ME vs. h curve is practically the same for all the four pressures investigated.

Cases 38-53 in Table 5 refer to a variation of the orifice diameter (namely, halving the base case scenario value (cases 38-45) and increasing it 1.5 times (cases 46-53)), while cases 54-73 involve a variation of both the storage pressure and the orifice diameter. From the corresponding plots (Figure 6.b and 7.c, respectively), we can see that the trends are similar to the ones found when varying the storage pressure (Figure 6.a). In particular, considering the same value of h, the larger the pressure or the orifice diameter are, the larger ME is. Therefore, the previous comments on the results in Figure 6.a hold true also for the ones in Figure 6.b and 6.c.

Considering cases 74-96, in Figure 6.d the results show the effect that different constant wind conditions have on the ME of the jet cloud for each wind profile used in the base case scenario. From this figure it is possible to observe how the wind intensity and shape modify the jet-ground interaction rather than the free jet characteristics. In fact, in terms of ME_{FJ}, all the results are within about 10% of the base case scenario, while in terms of h*, the range in which the results

vary is equal to about 50% of the base case scenario. In particular, the larger the wind velocity is, the smaller the h* is. Looking at the results influenced by the ground, two wind effects were identified: i) the lifting effect and ii) the stretching effect. The former acts by limiting the jet development toward the ground allowing greater air entrainment that leads to a reduction of the jet cloud's extent. The latter acts by increasing the extent of the jet in the axial direction because of the velocity of the flow field surrounding the jet. Two distinct situations can be highlighted: i) when the jet is close to the ground, the jet attaches quickly to it excluding the lifting effect. In this case only the contribution of the stretching effect is noticeable (the larger the wind velocity is, the larger the corresponding ME is); ii) when the jet is quite high over the ground, but still within the ground influence region, both effects are present.

For the purposes of comparison, in cases 97-132 the same constant wind conditions of tests 74-96 were considered together with a lower storage pressure.

In regard to cases 133-161, in which the influence of the pseudo-source was tested, Figure 6.f shows some dependence on the pseudo-source model. Since the same mass flow rate was used, the model of Yuceil and Otugen (2002), which predicts a smaller (nearly 2 times) equivalent diameter, leads to a much higher exit velocity and therefore to larger differences compared to the base case scenario. On the other hand, the pseudo-source model of Ewan and Moodie (1986) predicts almost the same equivalent diameter, leading to results that practically overlap the ones of the base case scenario. The results of this sensitivity are noticeably coherent with the findings reported by Franquet et al. (2015).

Table 5: Specifics and simulations settings.

case	p [bara]	T [K]	d [m]	d_{PS} model	v_z [m/s]	T_{amb} [K]	h [m]	
14-21	2.5	278	0.0254	Birch et al. (1984)	profile	300	0.028, 0.085, 0.143, 0.257, 0.314, 0.371, 0.486, 0.858	Figure 6.a
22-29	32.5	278	0.0254	Birch et al. (1984)	profile	300	0.103, 0.309, 0.515, 0.927, 1.134, 1.340, 1.752, 3.09	
30-37	130	278	0.0254	Birch et al. (1984)	profile	300	0.206, 0.618, 1.03, 1.855, 2.268, 2.680, 3.505, 6.186	
38-45	65	278	0.0127	Birch et al. (1984)	profile	300	0.073, 0.218, 0.364, 0.656, 0.802, 0.947, 1.239, 2.187	Figure 6.b
46-53	65	278	0.0381	Birch et al. (1984)	profile	300	0.218, 0.656, 1.093, 1.968, 2.405, 2.843, 3.717, 6.56	
54-57	20	278	0.0381	Birch et al. (1984)	profile	300	0.363, 0.849, 1.576, 3.153	Figure 6.c
58-61	30	278	0.01907	Birch et al. (1984)	profile	300	0.223, 0.520, 0.967, 1.934	
62-65	85	278	0.0127	Birch et al. (1984)	profile	300	0.250, 0.583, 1.084, 2.168	
66-69	120	278	0.0127	Birch et al. (1984)	profile	300	0.297, 0.693, 1.288, 2.576	
70-73	120	278	0.0381	Birch et al. (1984)	profile	300	0.891, 2.080, 3.863, 7.727	

74-80	65	278	0.0254	Birch et al. (1984)	1	300	0.3, 0.729, 1, 1.458, 1.895, 2.187	Figure 6.d
81-88	65	278	0.0254	Birch et al. (1984)	10	300	0.3, 0.729, 1, 1.458, 1.676, 1.895, 2.187, 6	
89-96	65	278	0.0254	Birch et al. (1984)	20	300	0.3, 0.729, 1, 1.312, 1.458, 1.895, 2.187, 6	
97-109	2.5	278	0.0254	Birch et al. (1984)	profile	300	0.028, 0.085, 0.143, 0.200, 0.257, 0.314, 0.371, 0.429, 0.486, 0.553, 0.6, 0.657, 0.858	Figure 6.e
110-116	2.5	278	0.0254	Birch et al. (1984)	1	300	0.143, 0.228, 0.3, 0.371, 0.429, 1, 6	
117-124	2.5	278	0.0254	Birch et al. (1984)	10	300	0.143, 0.228, 0.3, 0.328, 0.371, 0.429, 1, 6	
125-132	2.5	278	0.0254	Birch et al. (1984)	20	300	0.143, 0.228 0.257, 0.3, 0.371, 0.429, 1, 6	
133-144	65	278	0.0254	Ewan and Moodie (1986)	profile	300	0.137, 0.412, 0.687, 1.236, 1.511, 1.786, 1.923, 2.061, 2.198, 2.335, 4.122	Figure 6.f
145-161	65	278	0.0254	Yuceil and Otugen (2002)	profile	300	0.085, 0.255, 0.425, 0.765 , 0.935, 1.105, 1.19, 1.275, 1.36, 1.445, 1.53, 1.615, 1.7, 1.87, 2.04, 2.55, 3.4	
162-177	101	293	0.00635	FLACS embedded model	Not specified	293	0.029, 0.088, 0.206, 0.368, 0.481, 0.794, 1.011, 1.615, 2.032, 2.551, 3.197, 4, 6, 8, 10, free jet	From Benard et al. (2016)
178-195	251	293	0.00635	FLACS embedded model	Not specified	293	0.048, 0.143, 0.238, 0.333, 0.591, 0.769, 0.989, 1.263, 1.603, 2.025, 2.548, 3.197, 4, 5, 6, 8, 10, free jet	
196-213	401	293	0.00635	FLACS embedded model	Not specified	293	0.059, 0.176, 0.294, 0.412, 0.559, 0.74, 0.964, 1.242, 1.586, 2.012, 2.539, 3.191, 4, 5, 6, 8, 10, free jet	
214-232	551	293	0.00635	FLACS embedded model	Not specified	293	0.069, 0.207, 0.345, 0.483, 0.621, 0.795, 1.011, 1.28, 1.614, 2.031, 2.549, 3.195, 4, 5, 6, 7, 8, 10, free jet	
233-252	701	293	0.00635	FLACS embedded model	Not specified	293	0.077, 0.231, 0.385, 0.538, 0.72, 0.949, 1.231, 1.58, 2.01, 2.54, 3.195, 4, 5, 6, 7, 8, 9, 10, 11, free jet	

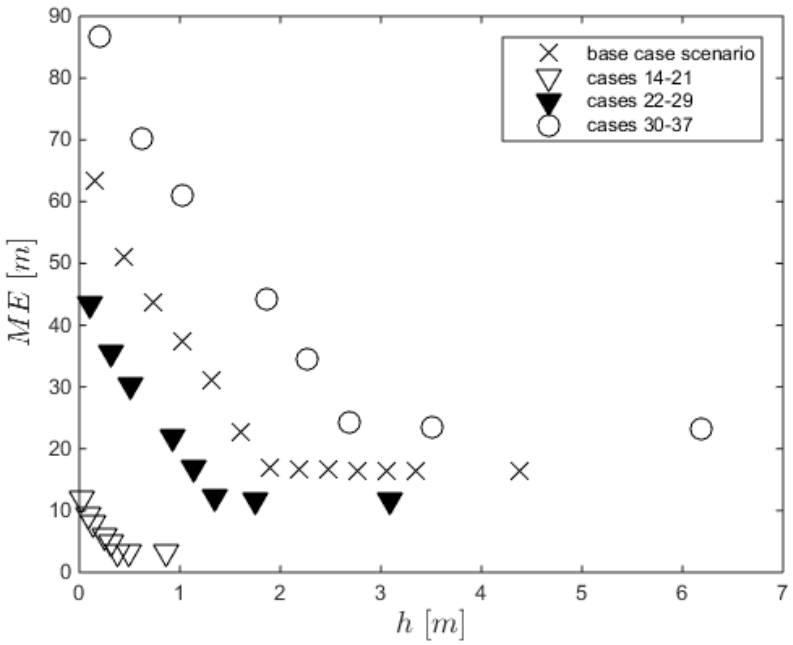

a

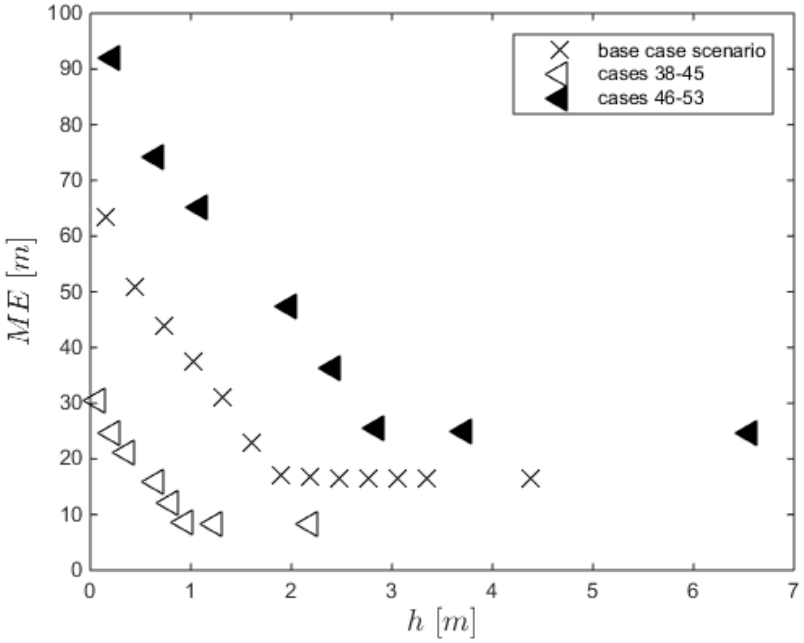
base case scenario
cases 38-45
cases 46-53
$ME\ [m]$
$h\ [m]$

b

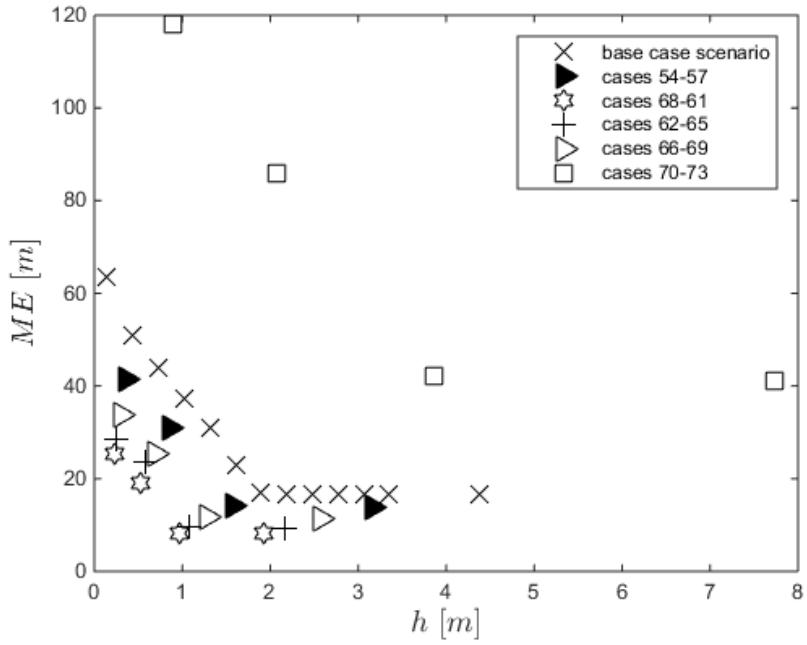
base case scenario
cases 54-57
cases 68-61
cases 62-65
cases 66-69
cases 70-73
$ME\ [m]$
$h\ [m]$

c

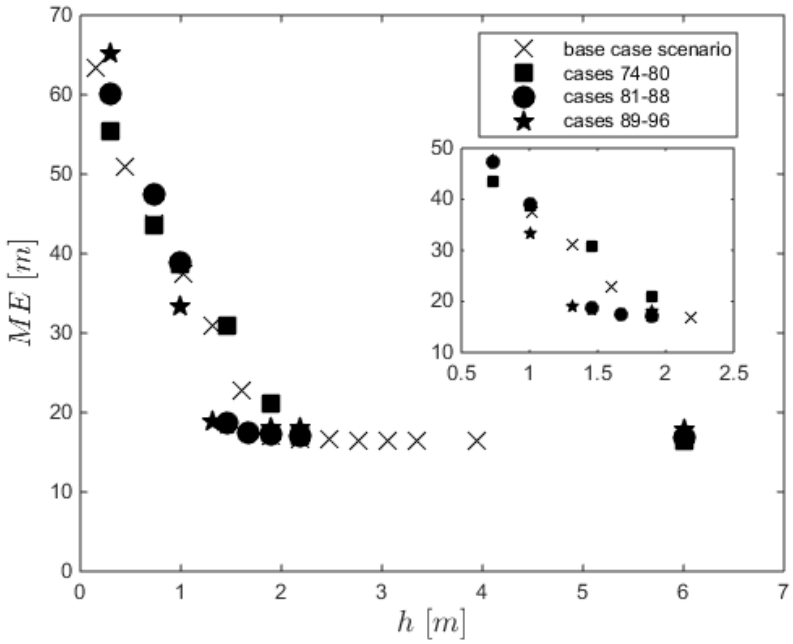
base case scenario
cases 74-80
cases 81-88
cases 89-96
$ME\ [m]$
$h\ [m]$

d

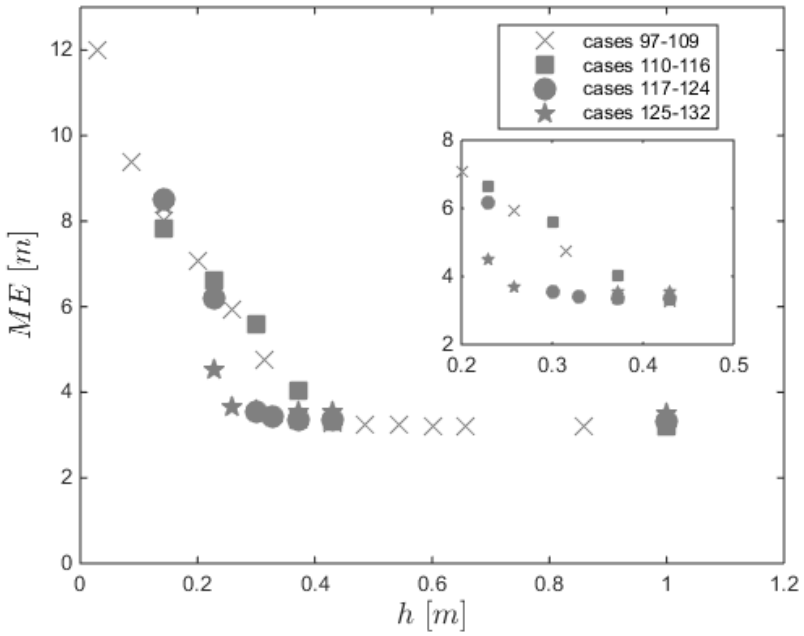
cases 97-109
cases 110-116
cases 117-124
cases 125-132
$ME\ [m]$
$h\ [m]$

e

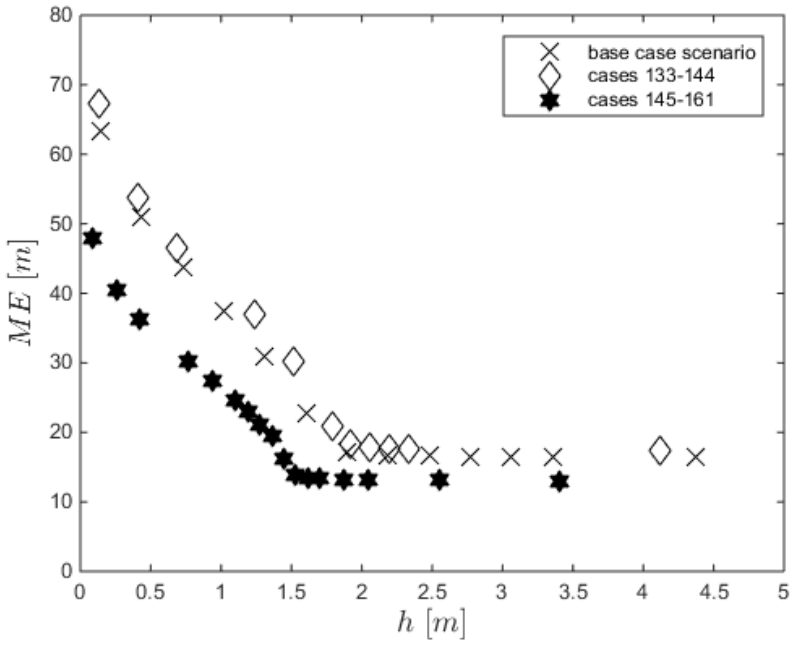

f

Fig. 6: ME vs. h for the base case scenario compared to those of the sensitivity analysis on (a) storage pressure, (b) actual orifice diameter, (c) storage pressure together with actual orifice diameter, (d) open field wind conditions, (e) open field wind conditions for a lower storage pressure (*i.e.*, 2.5 bara) and, (f) pseudo-source model.

Figures 6.a-f clearly show a substantial variability among the collected results. However, when replotted on the dimensionless space of Figure 5, all the results collapse on the same two lines (*i.e.*, the one due to the ground influence and the one of free jet behaviour) as shown in Figure 7 that, for the purposes of comparison, also reports some data from Benard et al. (2016) (cases 162-252 in Table 5).

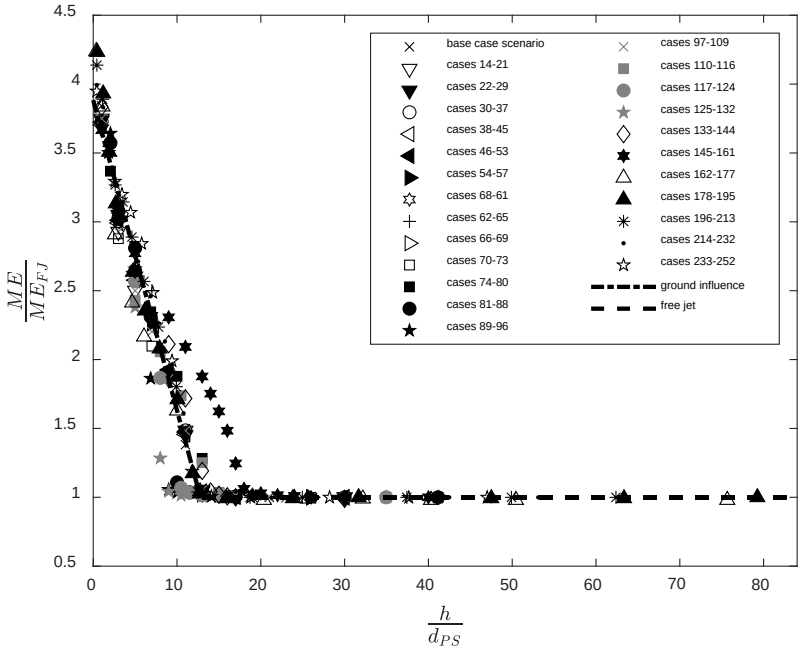

Fig. 7: Dimensionless ME vs. dimensionless height of the source above ground for all the cases investigated in the sensitivity analysis.

From this Figure, we can see that almost all the results overlap well the analytical correlation that models the ground influence and match the threshold value that limits its influence. Only the results obtained using the pseudo-source model of Yuceil and Otugen (2002) are underestimated by the analytical correlation for the ground influence when h/d_{PS} approaches $(h/d_{PS})^*$.

3.3 ME FREEJET ESTIMATION

The wide range validity of both the criterion and correlation proposed was verified through an extensive sensitivity analysis. To achieve such a validity extent, the ME_{FJ} estimation is one of the key parameters needed. For each of the scenarios considered, the ME of the free jet was computed by means of CFD simulation. However, ME_{FJ} can be also evaluated in a simpler way, such as using the analytical correlation developed by Chen and Rodi (1980) with d_{PS} substituted for the actual orifice diameter, d:

$$\eta = \frac{k d_{PS}}{z + a}\left(\frac{\rho_a}{\rho_g}\right)^{\frac{1}{2}} \tag{3}$$

Where η is the mean axial mole fraction, d_{ps} is the pseudo-source diameter, a is the virtual orifice displacement, k is the axial decay constant, z is the downstream distance, and ρ_a and ρ_g are the air and methane density, respectively.

Figure 8 compares the mole fraction axial decay predicted using this analytical correlation and the CFD model.

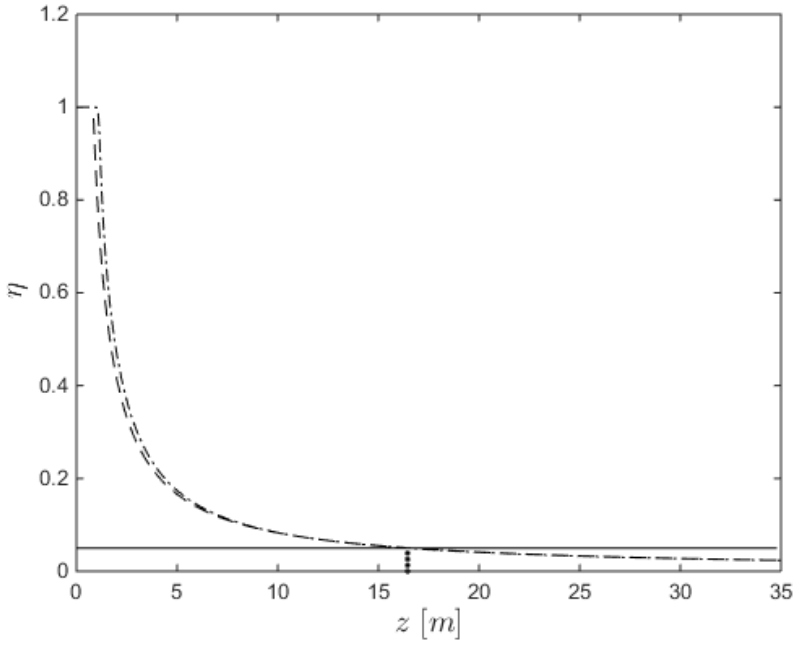

Fig. 8: Comparison of the methane mole fraction axial decay computed with the CFD model (dashed-dotted line) and the Chen and Rodi (1980) analytical model (dashed line), for the base case scenario. The solid line represents the mole fraction equal to the LFL (0.05) and the dotted line the corresponding ME_{FJ} (16.45 m) computed using the CFD model.

We can see that the models show no remarkable differences; at the LFL, the ME_{FJ} predicted by the CFD model is equal to 16.45 m, while the one given by the analytical model (considering an axial decay constant value of 4.4) is 0.8 % shorter.

Using the values of ME_{FJ} computed with Eq. 3, the results summarised in Figure 7 were plotted again in Figure 9. As shown in the previous Section, different pseudo-source models predict different pseudo-source diameter values, and consequently different ME_{FJ} values are computed. Therefore, Figure 9 includes the results having d_{PS} and ME_{FJ} values computed using the pseudo-source model of Birch et al. (1984). As expected, no significant differences compared to Figure 7 are evident, therefore allowing the use of Eq. 3 for estimating the ME_{FJ} value.

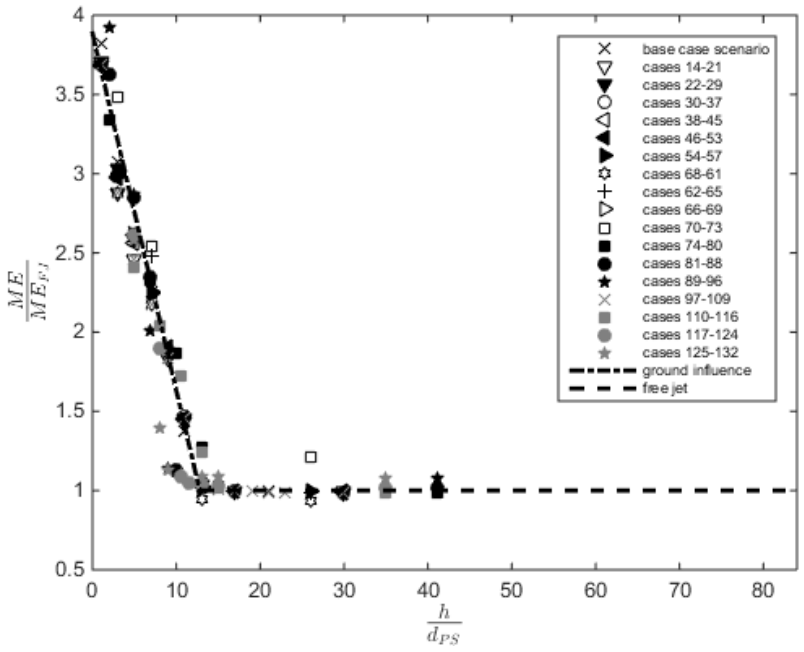

Fig. 9: Dimensionless ME vs. dimensionless height of the source above ground for all the cases investigated in the sensitivity analysis.

However, we can see that results computed for cases 70-73 do not follow the predicted behaviour as do the other results. There are two reasons for this: i) in these cases the LFL free jet cloud is substantially larger than that of the others (see Figure 6.c) and, ii) by Figure 8, for large distances from the jet source a high sensitivity of the ME_{FJ} on the model used is expected (the larger the distance from the jet source is, the closer the behaviour of the predicted mole fraction decay to the asymptotic value is).

4. CONCLUSIONS

As a matter of fact, the methane high-pressure gaseous release is a relevant safety-related problem mainly in the Oil and Gas (O&G) industry. In risk assessment, the damage area of the jet cloud (in particular, the hazardous distance reached by the LFL concentration value when the released compound is a flammable) is usually assumed as the hazardous distance to be estimated.

To estimate the maximum axially-oriented extent of the flammable cloud, the availability of reliable as well as simple, fast and easy-to-use tools for use in daily work is of primary importance. Focusing on the scenario of a high-pressure unignited methane jet outflowing from an accidental loss of containment close to the ground, the present work proposes a simple procedure that can be done by hand and enables safety analysts to estimate the hazardous distance.

The procedure can be summarised in the following steps:

1. From the accidental release characteristics, estimate the d_{PS} value using the Birch et al. (1984) model:

$$d_{PS} = d\sqrt{C_D\left(\frac{p}{p_{amb}}\right)\left(\frac{2}{\gamma+1}\right)^{\frac{(\gamma+1)}{2(\gamma-1)}}}$$

2. Estimate the ME_{FJ} value using the Chen and Rodi (1980) model:

$$ME_{FJ} = \frac{kd_{PS}}{LFL}\left(\frac{\rho_a}{\rho_g}\right)^{\frac{1}{2}}$$

3. If $h/d_{PS} > 13$, ME_{FJ} provides directly the order of magnitude of ME
4. If $h/d_{PS} < 13$, the order of magnitude of ME can be estimated as

$$ME = ME_{FJ}\left(3.89 - 0.22\frac{h}{d_{PS}}\right)$$

Finally, it should be stressed that this procedure is expected to provide a reasonable estimation as an order of magnitude of ME only inside the parameter window investigated. The use of detailed CFD simulations should be always considered both for confirming the estimated values, and for obtaining more reliable estimation in highly sensitive scenarios.

COMPETING INTERESTS STATEMENT

The Authors declare that there is no conflict of interest.

ACKNOWLEDGEMENTS

This research did not receive any specific grant from funding agencies in the public, commercial, or not-for-profit sectors.

REFERENCES

Ansys DesignModeler User's Guide, 2017. Release 19.0. ANSYS, Inc.

Ansys Fluent User's Guide, 2017. Release 19.0. ANSYS, Inc.

Ansys Meshing User's Guide, 2017. Release 19.0. ANSYS, Inc.

Alves, J.J.N., Neto, A.T.P., Araújo, A.C.B., Silva, H.B., Silva, S.K., Nascimento, C.A., Luiz, A.M., 2019. Overview and Experimental Verification of Models to Classify Hazardous Areas. *Process Saf. Environ. Prot.* 122, 102–17. https://doi.org/10.1016/j.psep.2018.11.021.

Angers, B., Hourri, A., Benard, P., Tchouvelev, A., 2011. Numerical investigation of a vertical surface on the flammable extent of hydrogen and methane vertical jets. *Int. J. Hydrogen Energy* 36, 2567-72.

Baalisampang, T., Abbassi, R., Garaniya, V., Khan, F., Dadashzadeh, M., 2019. Accidental release of Liquefied Natural Gas in a processing facility: Effect of equipment congestion level on dispersion behaviour of the flammable vapour. *J. Loss Prev. Process Ind.* 61, 237–248. https://doi.org/10.1016/j.jlp.2019.07.001.

Bariha, N., Srivastava, V.C., Mishra, I.M., 2017. Theoretical and experimental stuDies on hazard analysis of LPG/LNG release: A review. *Rev. Chem. Eng.* 33, 387–432. https://doi.org/10.1515/revce-2016-0006.

Batt, R., Gant, S.E., Lacome, J.M., Truchot, B., 2016. Modelling of stably-stratified atmospheric boundary layers with commercial CFD software for use in risk assessment. *Chem. Eng. Trans.* 48, 61–66. https://doi.org/10.3303/CET1648011.

Bénard, P., Tchouvelev, A., Hourri, A., Chen, Z., Angers, B., 2007. High pressure hydrogen jets in the presence of a surface. *Int. Conf. Hydrog. Saf.* 40.

Bénard, P., Hourri, A., Angers, B., Tchouvelev, A., Agranat, V., 2009. Effects of surface on the flammable extent of hydrogen jets. *Int. Conf. Hydrog. Saf*.

Bénard, P., Hourri, A., Angers, B., Tchouvelev, A., 2016. Adjacent surface effect on the flammable cloud of hydrogen and methane jets: Numerical investigation and engineering correlations. *Int. J. Hydrogen Energy* 41, 18654–18662. https://doi.org/10.1016/j.ijhydene.2016.08.173.

Birch, A.D., Brown, D.R., Dodson, M.G., Swaffield, F., 1984. The structure and concentration decay of high pressure jets of natural gas. *Combust. Sci. Technol.* 36, 249–261. https://doi.org/10.1080/00102208408923739.

Cameron, I., Raman, R., 2005. Process System Risk Management, first ed. Elsevier Amsterdam.

Casal, J., Gómez-Mares, M., Muñoz, M., Palacios, A., 2012. Jet fires: A 'minor' fire hazard? *Chem. Eng. Trans.* 26, 13–20. https://doi.org/10.3303/CET1226003.

Chen, C.J., Rodi, W., 1980. Vertical Turbulent Buoyant Jets – A review of Experimental Data, First ed. Pergamon Press Vol. 4.

Colombini, C., Busini, V., 2019. Obstacle Influence on High-Pressure Jets based on Computational Fluid Dynamics Simulations. *Chem. Eng. Trans.* 77, 811–816. https://doi.org/10.3303/CET1977136.

Colombini, C., Busini, V., 2019. High-Pressure Methane Jet: Analysis of the Jet-Obstcle Interaction. *Proceeding of the 29th European Safety and Reliability Conference.*

Crist, S., Sherman, P.M., Glass, D.R., 1966. Study of the highly underexpanded sonic jet. *AIAA J.* 4, 68–71. https://doi.org/10.2514/3.3386.

Dasgotra, A., Varun Teja, G. V.V., Sharma, A., Mishra, K.B., 2018. CFD modeling of large-scale flammable cloud dispersion using FLACS. *J. Loss Prev. Process Ind.* 56, 531–536. https://doi.org/10.1016/j.jlp.2018.01.001.

Deng, Y., Hu, H., Yu, B., Sun, D., Hou, L., Liang, Y., 2018. A method for simulating the release of natural gas from the rupture of high-pressure pipelines in any terrain. *J. Hazard. Mater.* 342, 418–428. https://doi.org/10.1016/j.jhazmat.2017.08.053.

Derudi, M., Bovolenta, D., Busini, V., Rota, R., 2014. Heavy gas dispersion in presence of large obstacles: Selection of modeling tools. *Ind. Eng. Chem. Res.* 53, 9303–9310. https://doi.org/10.1021/ie4034895.

Desilets, S., Cote, S., Nadau, G., Benard, P., Tchouvelev, A., 2009. Experimental results and comparison with simulated data of a low pressure hydrogen jet. *Int. Conf. Hydrog. Saf*.

Dey, S., Kishore, G.R., Castro-Orgaz, O., Ali, S.Z., 2017. Hydrodynamics of submerged turbulent plane offset jets. *Phys. Fluids* 29. https://doi.org/10.1063/1.4989559.

DNV, *PHAST - Process Hazard Analysis Software Tool,* DNV Software, last access: 27/03/2020. https://www.dnvgl.com/services/process-hazard-analysis-software-phast-1675

Efthimiou, G.C., Andronopoulos, S., Tavares, R., Bartzis, J.G., 2017. CFD-RANS prediction of the dispersion of a hazardous airborne material released during a real accident in an industrial environment. *J. Loss Prev. Process Ind.* 46, 23–36. https://doi.org/10.1016/j.jlp.2017.01.015.

Ewan, B.C., Moodie, K., 1986. Combustion Science and Technology Structure and Velocity Measurements in Underexpanded Jets Structure and Velocity Measurements in Undenexpanded Jets. *Combust. Sci. Tech* 4586, 275–288. https://doi.org/10.1080/00102208608923857.

Franquet, E., Perrier, V., Gibout, S., Bruel, P., 2015. Free underexpanded jets in a quiescent medium: A review. *Prog. Aerosp. Sci.* 77, 25–53. https://doi.org/10.1016/j.paerosci.2015.06.006.

Gerbec, M., Pontiggia, M., Antonioni, G., Tugnoli, a., Cozzani, V., Sbaouni, M., Lelong, R., 2017. Comparison of UDM and CFD simulations of a time varying release of LPG in geometrical complex environment. *J. Loss Prev. Process Ind.* 45, 56–68. https://doi.org/10.1016/j.jlp.2016.11.020.

Hall, J.E., Hooker, P., O'Sullivan, L., Angers, B., Hourri, A., Benard, P., 2017. Flammability profiles associated with high-pressure hydrogen jets released in close proximity to surfaces. *Int. J. Hydrogen Energy* 42, 7413–7421. https://doi.org/10.1016/j.ijhydene.2016.05.113.

Hendrickson, B., Marsegan, C., Gavelli, F., 2016. Where to begin – A parametric study for vapor barriers at LNG export facilities. *J. Loss Prev. Process Ind.* 44, 573–582. https://doi.org/10.1016/j.jlp.2016.07.031.

Houf, W., Schefer, R., Evans, G., Merilo, E., Groethe, M., 2010. Evaluation of barrier walls for mitigation of unintended releases of hydrogen. *Int. J. Hydrogen Energy* 35, 4758–4775. https://doi.org/10.1016/j.ijhydene.2010.02.086.

Hourri, A., Angers, B., Bénard, P., 2009. Surface effects on flammable extent of hydrogen and methane jets. *Int. J. Hydrogen Energy* 34, 1569–1577. https://doi.org/10.1016/j.ijhydene.2008.11.088.

Hourri, A., Angers, B., Bénard, P., Tchouvelev, A., Agranat, V., 2011. Numerical investigation of the flammable extent of semi-confined hydrogen and methane jets. *Int. J. Hydrogen Energy* 36, 2567–2572. https://doi.org/10.1016/j.ijhydene.2010.04.121.

Jiang, Y., Xu, Z., Wei, J., Teng, G., 2020. Fused CFD-interpolation model for real-time prediction of hazardous gas dispersion in emergency rescue. *J. Loss Prev. Process Ind.* 63, 103988. https://doi.org/10.1016/j.jlp.2019.103988.

Kim, S., Lee, H.J., Park, J.H., Jeung, I.S., 2013. Effects of a wall on the self-ignition patterns and flame propagation of high-pressure hydrogen release through a tube. *Proc. Combust. Inst.* 34, 2049–2056. https://doi.org/10.1016/j.proci.2012.09.001.

Kong, X.X., Wang, X.S., Cong, H.Y., Liu, Y.P., Zhu, J.P., 2019. Temperature profile and flame extension length of a ceiling impinging round jet fire in an inclined tunnel. *Int. J. Therm. Sci.* 137, 526–533. https://doi.org/10.1016/j.ijthermalsci.2018.12.023.

Kotchourko, A., Baraldi, D., Bénard, P., Eisenreich, N., Jordan, T., Keller, J., Kessler, A., LaChance, J., Molkov, V., Steen, M., Tchouvelev, A., 2014. State of the Art and Research Priorities in Hydrogen Safety. Joint Research Centre of the European Commission (JRC), Honolulu, Hawaii.

Liao, N., Huang, K., Chen, L., Wang, Z, Wu, J., Zhang, F., 2018. Numerical simulation of gas dispersion during cold venting of natural gas pipelines. *Adv. Mech. Eng.* 10, 1–14. https://doi.org/10.1177/1687814018755244.

Lim, J.W., Baalisampang, T., Garaniya, V., Abbassi, R., Khan, F., Ji, J., 2019. Numerical analysis of performances of passive fire protections in processing facilities. *J. Loss Prev. Process Ind.* 62,

103970. https://doi.org/10.1016/j.jlp.2019.103970.

Luo, T., Yu, C., Liu, R., Li, M., Zhang, J., Qu, S., 2018. Numerical simulation of LNG release and dispersion using a multiphase CFD model. *J. Loss Prev. Process Ind.* 56, 316–327. https://doi.org/10.1016/j.jlp.2018.08.001.

Menter, F.R., 1993. Zonal Two Equation kω Turbulence Models for Aerodynamic Flows. *24th Fluid Dynamics Conference*.

Middha, P., Hansen, O.R., Grune, J., Kotchourko, A., 2010. CFD calculations of gas leak dispersion and subsequent gas explosions: Validation against ignited impinging hydrogen jet experiments. *J. Hazard. Mater.* 179, 84–94. https://doi.org/10.1016/j.jhazmat.2010.02.061.

Miozzi, M., Lalli, F., Romano, G.P., 2010. Experimental investigation of a free-surface turbulent jet with Coanda effect. *Exp. Fluids* 49, 341–353. https://doi.org/10.1007/s00348-010-0885-1.

Pontiggia, M., Derudi, M., Busini, V., Rota, R., 2009. Hazardous gas dispersion: A CFD model accounting for atmospheric stability classes. *J. Hazard. Mater.* 171, 739–747. https://doi.org/10.3303/CET1436088.

Pontiggia, M., Busini, V., Ronzoni, M., Uguccioni, G., Rota, R., 2014. Effect of large obstacles on high momentum jets dispersion. *Chem. Eng. Trans.* 36, 523–528. https://doi.org/10.1016/j.jhazmat.2009.06.064.

Pu, L., Tang, X., Shao, X., Lei, G., Li, Y., 2019. Numerical investigation on the difference of dispersion behavior between cryogenic liquid hydrogen and methane, *Int. J. Hydrogen Energy* 44, 22368-22379.

Schleder, A.M., Pastor, E., Planas, E., Martins, M.R., 2015. Experimental data and CFD performance for cloud dispersion analysis: The USP-UPC project. . *J. Loss Prev. Process Ind.* 38, 125-138.

Souza, A. O. *et al.* A new correlation for hazardous area classification based on experiments and CFD predictions. *Process Saf. Prog.* 38, 21–26 (2019). https://doi.org/10.1002/prs.11974.

Stewart, J.R., 2019. CFD modelling of underexpanded hydrogen jets exiting rectangular shaped openings. *Inst. Chem. Eng. Symp. Ser.* 2019-May.

Tchouvelev, A.V., Cheng, Z., Agranat, V.M., Zhubrin, S.V., 2007. Effectiveness of small barriers as means to reduce clearance distances. *Int. J. Hydrogen Energy* 32, 1409–1415. https://doi.org/10.1016/j.ijhydene.2006.10.020.

Tolias, I. C., Giannissi, S.G., Venetsanos, A.G., Keenan, J., Shentsov, V., Makarov, D., Coldrick, S., Kotchourko, A., Ren, K., Jedicke, O., Melideo, D., Baraldi, D., Slater, S., Duclos, A., Verbecke, F., Molkov, V., 2019. Best practice guidelines in numerical simulations and CFD benchmarking for hydrogen safety applications. *Int. J. Hydrogen Energy* 44, 9050–9062. https://doi.org/10.1016/j.ijhydene.2018.06.005.

Uggenti, A.C., Carpignano, A., Savoldi, L., Zanino, R., 2017. Perspective and criticalities of CFD

modelling for the analysis of oil and gas offshore accident scenarios. *Risk, Reliability and Safety: Innovating Theory and Practice: Proceedings of ESREL 2016.*

Xu, B.P., Wen, J.X., Tam, V.H.Y., 2011. The effect of an obstacle plate on the spontaneous ignition in pressurized hydrogen release: A numerical study. *Int. J. Hydrogen Energy* 36, 2637–2644. https://doi.org/10.1016/j.ijhydene.2010.03.143.

Yang, R., Khan, F., Taleb-Berrouane, M., Kong, D., 2020. A time-dependent probabilistic model for fire accident analysis. *Fire Saf. J.* 111, 102891. https://doi.org/10.1016/j.firesaf.2019.102891.

Yüceil, K.B., Ötügen, M.V., 2002. Scaling parameters for underexpanded supersonic jets. *Phys. Fluids* 14, 4206–4215. https://doi.org/10.1063/1.1513796.

Zhou, K., Wang, X., Liu, M., Liu, J., 2018. A theoretical framework for calculating full-scale jet fires induced by high-pressure hydrogen/natural gas transient leakage. *Int. J. Hydrogen Energy* 43, 22765–22775. https://doi.org/10.1016/j.ijhydene.2018.10.122.